LINKIN-associated proteins necessary for tissue integrity during collective cell migration

Chieh-Hsiang Tan[1]*, Kai-Wen Cheng[1,] *, Heenam Park, Paul W. Sternberg[1#] and Tsui-Fen Chou[1,2#]

1: Division of Biology and Biological Engineering, California Institute of Technology;

2: Proteome Exploration Laboratory, Beckman Institute, California Institute of Technology

*denotes equal contribution; # for correspondence

Emails:

Chieh-Hsiang Tan: chtan@caltech.edu

Kai-Wen Cheng: kwcheng.taiwan@gmail.com

Heenam Park: heenam@caltech.edu

Tsui-Fen Chou: tfchou@caltech.edu

Paul W. Sternberg: pws@caltech.edu

ORCID:

Chieh-Hsiang Tan: 0000-0002-5432-0160

Kai-Wen Cheng: 0000-0001-9888-9773

Heenam Park: 0000-0001-7911-5828

Tsui-Fen Chou: 0000-0003-2410-2186

Paul W. Sternberg: 0000-0002-7699-0173

Abstract

Cell adhesion plays essential roles in almost every aspect of metazoan biology. Previously, using the developmental migration of the nematode male gonad as a platform, LINKIN (Human: ITFG1, *C. elegans*: *lnkn-1*), a relatively understudied transmembrane protein conserved across the metazoa, was found to be necessary for tissue integrity during migration. In *C. elegans*, loss of *lnkn-1* results in the detachment of the lead migratory cell from the rest of the developing male gonad. Three interactors of ITFG1/*lnkn-1*- RUVBL1/*ruvb-1*, RUVBL2/*ruvb-2*, and alpha-tubulin were identified by proteomic analysis using the human HEK293T cells and validated in the nematode male gonad. The ITFG1-RUVBL1 interaction has since been independently validated in a breast cancer cell line model that also implicates the involvement of the pair in metastasis. In this study, we showed that epitope-tagged ITFG1 localized to the cell surface of MDA-MB-231 breast cancer cells. Using unbiased mass spectrometry-based proteomics, we identified a new list of potential interactors of ITFG1. *Loss-of-function* analysis of their *C. elegans* orthologs found that three of the interactors- ATP9A/*tat-5*, NME1/*ndk-1*, and ANAPC2/*apc-2* displayed migratory detachment phenotypes similar to that of *lnkn-1*. Taken together with the other genes whose reduction of function phenotype is the same as LINKIN (notably cohesion and condensin) suggests the involvement of membrane remodeling and chromosome biology in the tight adhesion dependent on LINKIN, and support the hypothesis for a structure role of chromosomes in post-mitotic cells.

Introduction

Cell adhesion is inherently involved in biological processes that extend to more than one cell. Biological process, including that of metazoan development and intercellular signal transduction, requires a fine-tuning of both the strength and the content of cell adhesion. As such, misregulation or alteration of cell adhesion proteins leads to a broad spectrum of pathological conditions (Hynes, 1999; Janiszewska et al., 2020). Abnormal cell adhesion is associated with cancer development. For a tumor to be metastatic, malignant cells must both acquire the ability to migrate and lose cell adhesion (Geiger and Peeper, 2009). Decades of research and the advancement of genetics and molecular biology has led to much knowledge of how cell adhesion is maintained, both in terms of mechanism as well as the molecules involved. However, questions remained, such as how dynamic cell adhesion is maintained during cell migration (Collins and Nelson, 2015).

The gonad of *Caenorhabditis elegans* is shaped through a combination of elongation and a stereotypic migration guided by a migratory leader cell. In male worms, the leader cell is a somatic gonadal cell known as the linker cell (LC) (Hirsh et al., 1976; Kimble and Hirsh, 1979; Klass et al., 1976). At the leading edge of the elongating male gonad, the migratory linker cell leads a collective migration followed by a stalk of passive migratory cells. There are many similarities between this collective migration and some of the well-known examples described in other organisms (Scarpa and Mayor, 2016), including the specification of the leader cell through Notch signaling (Greenwald et al., 1983; Yochem et al., 1988). However, as typical with nematode development, the cell fate of the linker cell and the followers commit early and are generally unexchangeable (Kimble, 1981). As with the leader cells in other collective migrations (Mayor and Etienne-Manneville, 2016), the linker cell is responsible for both determining the direction of the migration (Kimble and Hirsh, 1979) and for generating a significant part of the traction forces “dragging” the group in the migration (Kato et al., 2014). If detached from the rest of the gonad, the linker cell retains the ability to migrate while the rest of the gonad cease to elongate (Chisholm, 1991; Kato et al., 2014; Sternberg and Horvitz, 1988). Maintaining the cell-to-cell adhesion under intense stress and, thus, the overall integrity of the migrating complex is all but essential for gonadogenesis. Therefore, the migrating male gonad in this

transparent nematode can be a good genetic model for the study of cell adhesion dynamics during migration.

A few proteins have been identified to be essential for tissue integrity and the cell adhesiveness of the linker cell-led collective migration. These include cytoskeleton protein- alpha-tubulin, TBA-2, and beta-tubulin, TBB-2; SMC proteins HIM-1, SMC-3, SMC-4; Homeobox transcription factor- EGL-5; AAA+ ATPase superfamily protein- RUVB-1, RUVB-2; and LNKN-1, a conserved but poorly characterized transmembrane protein (Chisholm, 1991; Kato et al., 2014; Schwarz et al., 2012). Based upon the expression profile of a similar cell (Hunt-Newbury et al., 2007), Kato et al. (2014) identified *lnkn-1* through the observation of a linker cell detachment phenotype. This was followed by a proteomic approach consisting of immunoprecipitation with the human *lnkn-1* ortholog ITFG1 and protein identification through mass spectrometry. The interactors of ITFG1 were then functionally assayed in the nematode model using RNA interference, thereby identifying TBA-2, TBB-2, RUVB-1, and RUVB-2 as sharing the highly specific linker cell detachment phenotype with LNKN-1 (Kato et al., 2014). The interaction between *lnkn-1*/ITFG1 and *ruvb-1*/RUVBL1 was later independently verified in a breast cancer cell line study (Fan et al., 2017), which also associates the pair with breast cancer progression.

In this study, we set out to identify other interactors of LNKN-1/ITFG1 to advance our understanding of its role in the adhesion of migratory cells. We started by identifying interactors of the human ITFG1 in the breast cancer cell line MDA-MB-23. The cell line selection was based on physiological/ pathological relevance and documented expression (Fan et al., 2017). Working with the same breast cancer cell line, we validated the ITFG1-RUVBL1 interaction and showed that ITFG1 is localized to the cell surface, consistent with it being responsible for cell adhesion. Through immunoprecipitation and mass spectrometry-based protein identification in ITFG1-expressing cells, 1756 and 373 potential interactors of ITFG1 were identified in ITFG1 transient and stably expressing cells, respectively. Of these, 180 were identified through two unbiased independent experimental setups. We then proceed to test the findings in *C. elegans*, in worms carrying loss-of-function mutations in their orthologs. We analyzed multiple phenotypes

observed in *lnkn-1* knock-out worms, including that of the linker cell migration. We identified four genes that resulted in worms with incomplete migrations, of which none have been previously identified with this phenotype: aminophospholipid translocase- *tat-5*/ATP9A; nucleoside diphosphate kinase- *ndk-1*/NME1; anaphase-promoting complex- *apc-2*/ANAPC2; and metastasis-associated protein- *lin-40*/MTA2. Like that of *lnkn-1* mutants, in worms carrying *tat-5*, *ndk-1*, or *apc-2* loss-of-function alleles, the migratory failure is likely caused by the disassociation of the linker cell from the majority of the elongating gonad. We conclude that they are likely some of the many components that control the tight connection of a migratory cell to its follower cells.

Results

Surface expression of ITFG1 on MDA-MB-231 cells

We generated ITFG1-expressing MDA-MB-231 cells by the transfection of full-length ITFG1 cDNA with a Myc tag at the C-terminal (ITFG1-Myc). Transfected cells of two biological replicates were harvested 48 hours post-transfection with non-transfected MDA-MB-231 cells serving as control. The ITFG1-Myc expression was confirmed by RT-qPCR, as a higher level of ITFG1 mRNA level was detected (Fig. 1A). We then validated cellular ITFG1 protein expression by immunoblot analysis using anti-Myc and anti-ITFG1 antibodies. As shown in Fig. 1B, protein bands with apparent molecular weight between 75 and 100 kDa were detected in transfected cells probed with anti-Myc and ani-ITFG1 antibodies but not in control cells, representing the overexpression of ITFG1 protein in ITFG1-Myc transfected cells. Moreover, to further confirm the molecular weight of ITFG1, immunoprecipitated proteins in the gel range around 150 to 250 kDa (R1 region), 75 to 150 kDa (R2 region), and 37 to 75 kDa (R3 region) were extracted, trypsin digested, and subjected for mass spectrometry analysis. A relatively high abundance of ITFG1 protein was identified in the gel range between 75 to 150 kDa (R2 region) and 37 to 75 kDa (R3 region) of extracts from transfected cells (Fig. S1). Conversely, ITFG1 protein was only identified in the gel range between 75 to 150 kDa (R2 region) of control cells, indicating the expression of endogenous ITFG1 protein in MDA-MB-231 cells.

To investigate the subcellular localization of ITFG1 protein in MDA-MB-231 cells, cell lysates obtained from ITFG1-Myc transfected cells were subcellular fractionated and subjected to immunoblot analysis. We also expressed ITFG1 in MDA-MB-231 as reference to exclude the interference of the Myc tag. We found that ITFG1 protein with or without Myc tag was primarily found in the membrane fraction, suggesting that the Myc tag does not alter the subcellular localization of (Fig. 1C). Immunostaining was also performed to confirm the membrane localization of ITFG1. We found, using an anti-ITFG1 antibody, that ITFG1 can be detected on the plasma membrane of transfected cells but not that of the control cells (Fig. 1D). Cell surface expression of ITFG1 in transfected cells was also confirmed by flow cytometry, while no surface ITFG1 was detected in control cells (Fig. 1E). Overall, we show that ITFG1 primarily localized to the plasm membrane in MDA-MB-231 cells, but the endogenous expression level is low.

Validation of ITFG1-RUVBL1 interactions

We sought to identify ITFG1 interactors in MDA-MB-231 cells to further our understanding of the function of ITFG1 in breast cancer. We established stable ITFG1-Myc-expressing MDA-MB-231 cells by lentivirus delivery, Cell lysates from both the transient and stable expression cultures were subjected to immunoprecipitation with anti-Myc agarose affinity gels followed by mass spectrometry, with MDA-MB-231 cells serving as control. Notably, mass spectrometry analysis shows that ITFG1 protein was 162.8-fold (log2 = 7.3) and 105.9-fold (log2 = 6.7) enriched in immunoprecipitated products of transient and stable ITFG1-Myc-expressing cells compared to control cells, respectively (Fig. 2A), confirming a successful immunoprecipitation coupled to mass spectrometry.

We then determined whether ITFG1 interacts with RUVBL1, an identified ITFG1 binding partner (Kato et al., 2014), including in the MDA-MB-231 cells (Fan et al., 2017). Mass spectrometry analysis shows that RUVBL1 protein was 26.8-fold (log2 = 4.7) and 6.09-fold (log2 = 2.6) enriched in immunoprecipitated products of transient and stable ITFG1-Myc-expressing cells, respectively, compared to control cells (Fig. 2B). Total cell lysates and immunoprecipitated factions from ITFG1-Myc transfected cells and control cells were subjected to immunoblot analysis for ITFG1 and RUVBL1. RUVBL1 was enriched in the

pulldown samples from transfected cells compared to control cells (Fig. 2C), supporting an interaction between ITFG1 and RUVBL1. We next transiently expressed RUVBL1 with a FLAG tag at the N-terminal (FLAG-RUVBL1) in ITFG1-Myc-expressing or control MDA-MB-231 cells, and subsequently performed immunoprecipitation from cell lysates using anti-Flag agarose affinity gels. The expression of ITFG1 and FLAG-RUVBL1 proteins were identified in ITFG1-Myc-expressing MDA-MB-231 cells by immunoblotting assays (Fig. 2D). All the pulldown products were examined for the presence of ITFG1 and FLAG-RUVBL1 by immunoblotting with anti-ITFG1 and anti-FLAG antibodies, respectively. As shown in Fig. 2D, FLAG-RUVBL1 co-purified with ITFG1 was only detected in lysates from ITFG1-myc-expressing cells with FLAG-RUVBL1 expression, indicating the binding of ITFG1 to RUVBL1. Taken together, these data confirm the known specific interaction of ITFG1 and RUVBL1, providing evidence of the validity of immunoprecipitation-mass spectrometry approach.

Function and pathway analysis of ITFG1 interactors

To discover ITFG1 interacting proteins, we performed mass spectrometry analysis to identify the proteins captured in the IP assay from transient and stable ITFG1-Myc-expressing MDA-MB-231 and control cells in two independent sets. As shown in Fig. 3A, we identified a total of 2628 and 1242 proteins with higher enrichment (log2 FC > 0.6) in transient and stable ITFG1-expressing cells over control cells, respectively (Table S1-2). To gain insight into their biological significance, we further compared the two sets of enriched proteins (Log2 FC > 2) and identified 180 proteins shared between ITFG1-Myc-expressing cells (Fig. 3B, Table S3), suggesting that they specifically associate with ITFG1 in MDA-MB-231 cells. We then performed gene ontology (GO) biological process and Reactome pathway enrichment analysis of these 180 proteins, and found that the ITFG1 interacting proteins were enriched in multiple cell networks, including cell cycle, mitochondria translation initiation, and regulation of DNA repair, among others. A total of 17 proteins primarily participating in cell cycle were identified (Table S4).

Mutations in the orthologs of ITFG1 interactors resulted in phenotypes similar to that of *lnkn-1* mutants

To validate the potential interactors and to explore their biological functions, we returned to the *C. elegans* model, where *lnkn-1* was originally identified (Kato et al., 2014). To select candidates for genetic analysis in this worm, we made our selection criteria more stringent, requiring candidates to be not only enriched in both sets of ITFG1 expressing cells but also detected in all of the individual samples and at least >2.5 log2 fold enriched on average in the stable ITFG1 expressing cell line. Based on these stringent criteria, 84 *C. elegans* orthologs of 78 candidates were identified (Table S5), including the expected *lnkn-1*/ITFG1 and the previously identified *ruvb-1*/RUVBL1, *ruvb-2*/RUVBL2.

We reasoned that if the worm orthologs of the candidates interact with LNKN-1 in the cell adhesion process in *C. elegans*, loss-of-function of their encoding genes should display a phenotype similar to that of *lnkn-1(lf)*. Kato et al. (2014) reported multiple phenotypes associated with *lnkn-1* loss-of-function allele *gk367*, including that of the linker cell detachment. The allele *gk367*, generated by the knock out consortium (Consortium, 2012), consists of a deletion that covers part of the *lnkn-1* coding sequence resulting in a truncated protein. Although the deletion only alters the coding sequence of *lnkn-1*, it is possible that *gk367* could also affect the expression of other genes co-transcribed in the same operon CEOP3552 (Davis et al., 2022). However, the phenotype observed in *gk367* animals is likely to resemble that of *lnkn-1(null)*, as the truncated protein is mislocalized (Kato et al., 2014), and knock-out of the next closest gene in the operon does not have similar effects (Tan et al., 2022). To generate a convincing single gene knockout we used the STOP-IN cassette strategy (Wang et al., 2018) to generate knock-out allele *sy1596* of *lnkn-1*; this was used for phenotypic analysis.

To select candidates for a comprehensive phenotypic analysis, we focused on genes that are likely to be essential. Hermaphrodites of both *lnkn-1(sy1596)* (Fig. 4) and *lnkn-1(gk256)* homozygous strains (Kato et al., 2014) are recessively maternal effect lethal; both *ruvb-1* and *ruvb-2* were also reported to be essential (Consortium, 2012; Updike and Mango, 2007). We reason that this is caused by the essentiality of a gene that is involved in the critical biological role of cell adhesion during development and that a significant

amount of genetic information is provided maternally during nematode development (Evans and Hunter, 2005; Miwa et al., 1980; Wood et al., 1980). Therefore, we obtained deletion alleles for candidate genes based on their availability and whether the allele was phenotypically characterized as either lethal or sterile. To simplify developmental and fertility analysis we wanted to avoid the aneuploidy generated by translocation balancers, and we thus rebalanced 19 lethal/sterile mutations primarily with the structurally defined and fluorescently and phenotypically labeled set of balancers described in Dejima et al. (2018) (Table S6). We then select 17 candidate genes (Fig. 4C), starting with phenotypic analysis in the hermaphrodites. In all cases, homozygous animals descended from balanced heterozygous mothers were identified through the lack of fluorescently labeled balancers (Fig. 4A). Mutants of seven candidate genes failed to develop into adults, arresting at various larval stages, preventing further characterization (Fig. 4C, phenotype 1). Of the these alleles, *feh-1(gb561)* (Zambrano et al., 2002), *trd-1(tm2764)* (Hughes et al., 2014), *hsp-1(ok1371)* (knock out consortium), and *hsp-90(ok1333)* (knock out consortium) were previously reported; while the phenotype of *mvk-1(tm6628)*, *vha-19(tm2225)*, and *prx-3(tm6469)* were previously unclear. Although not followed up upon, it is entirely possible that these genes also contribute to LNKN-1-associated cell adhesion. The mutant animals from the rest of the selected candidates were able to develop successfully into adults (Fig. 4C phenotype 1), and we followed up the analysis with a focus on fertility. As expected, most candidates failed to produce progeny that hatched, similar to *lnkn-1* loss-of-functions (Fig. 4C phenotype 2; (Kato et al., 2014). A major exception is *cdc-25.2(ok597)*, which we found to be fertile, consistent with a previous observation of low penetrance fertility (Kim et al., 2010). Another is that of *lin-40*, in which the *gk255* allele was selected for analysis based on the severity of the sterile phenotype we observed- *gk255* is maternal effect sterile while two other deletion alleles *ok905* and *ok906* were fertile. Unmated *lnkn-1(sy1596)* hermaphrodites produce a small number of oocytes and embryos that fail to hatch (Fig. 4C, phenotype 3). To test whether the embryonic contribution of LNKN-1 can alleviate this lethality, we cross the *lnkn-1(sy1596)* hermaphrodites with wild-type males with fluorescent genetic markers (Fig. 4A). The cross generates embryos with the male-derived fluorescent marker that still failed to hatch (Fig. 4B; Fig. 4C, phenotype 4,5), indicating that LNKN-1 is required in embryogenesis

and to be provided maternally. Assessing the mutants of the candidate genes based on the *lnkn-1* phenotype mentioned above (Fig. 4C, phenotype 3,4,5), we find that *tat-5(tm1741)* and an uncharacterized gene *C10B5.1(ok3270)* is phenotypically similar to *lnkn-1*. *rad-51(ok2218)* and *vps-41(ok3433)* produced embryos that failed to hatch, and we were unable to obtain cross embryos through mating. On the other hand, although *unc-94(ok1210)* hermaphrodites rarely lay embryos or unfertilized oocytes by themselves (although it does produce them), it was able to produce mated heterozygotic animals that hatch. Suggesting that UNC-94 can be supplied both embryonically and maternally, a major difference from that of LNKN-1. No embryos or oocytes were observed outside of the animal for *cdc-25.1(ok1888)*, *ndk-1(ok314)*, *apc-2(ok1657)*, and *rod-1(tm6186)*, and no mating resulted in cross progeny.

Hermaphrodite gonad development has much in common with that of the male but with a few clear distinctions: 1) In *C. elegans*, the hermaphrodite gonad is two-armed compared with one in the male and 2) the gonads of both males and hermaphrodites can be conceptualized as tubes with a directional axis defined by the maturation of the germ cells, which occurs from distal to proximal (Kimble and Hirsh, 1979). The major difference is in the direction in which the gonad elongates, at the proximal end in males and the distal ends in hermaphrodites. 3) Partially as a consequence of the flip in the elongating direction, different cells serve the role of determining the migratory direction. On the proximal end, the linker cell (LC) serves as the leader cell in the migratory process. It both determines the direction of the migration and actively contributes to the process (Kato et al., 2014; Kimble and Hirsh, 1979). In hermaphrodites, with the primary elongation occurring at the other end of the tube, the cell that can be considered analogous to the linker cell – the anchor cell (AC) – is instead responsible for the induction of the vulva in the adjacent epidermal tissue (Kimble, 1981). Both cells are essential in their respective sexes in connecting the gonadal lumen to the exterior opening. In addition, in some other nematodes, the anchor cell also has a migratory role similar to the male linker cell (Felix and Sternberg, 1996). On the distal end, distal tip cells (DTC), two in the single-armed male gonad and one each in the two-armed hermaphrodite gonads, maintains the stem cell niche from which the germ cells proliferate (Kimble and White, 1981). In hermaphrodites, whereas the gonad elongation occurs at the distal end, the distal cells

are also responsible for determining the migratory direction (Kimble and White, 1981), playing a role similar to that of the linker cell in the males. However, different from that of the linker cell, the distal tip cell does not in itself provides the traction for the migration, instead relying on the forces generated by the proliferating germ cells pushing it forward (Agarwal et al., 2022).

The gonads of *lnkn-1(sy1596)* hermaphrodites were noticeably different in shape from that of the wild-type (Fig. 5A, B), a phenotype that was also previously noted in *lnkn-1(gk255)* (Kato et al., 2014). The two U shaped gonad arm of the hermaphrodites can be roughly divided into two halves each- The ventral-proximal half, which connects to the vulval and is shaped by the earlier centrifugal migration; and the dorsal-distal half, which is capped by the distal tip cell and is shaped by the later centripetal migration. In *lnkn-1(sy1596)* hermaphrodites, the centripetal half of the gonad is significantly shorter proportional-wise compared to that of the wild-type (Fig. 5). This difference might be caused by either a late ventral to dorsal turn during the migration or that of a premature stop near the end of the elongation process. We examined the nine sterile (Fig. 4 phenotype 2) candidates for similarities in morphology and found six of them, *cdc-25.1*, *tat-5*, *ndk-1*, *apc-2*, *rod-1*, and *C10B5.1,* share the phenotype. The phenotype has been previously reported in *ndk-1* and *apc-2* (Cram et al., 2006; Fancsalszky et al., 2014). Since the migration and elongation of the hermaphrodite gonad are driven by germ cell proliferation, and most if not all of the candidates produce much fewer embryos/ embryo-like objects compared to that of the wild-type, it is likely that at least part of the premature stopping could be due to reduced germ cell proliferation at later developmental stages. Indeed, one of the six candidates, namely *cdc-25.1* has been found to be required for germ cell proliferation and is described to have a reduced-sized gonad (Ashcroft and Golden, 2002; Kim et al., 2009; Yoon et al., 2012). It is worth noting that, similar to that of *lnkn-1*, all nine candidates have an overall reduced gonad size, but only six stop prematurely in the centripetal migration, so there are likely other factors involved.

TAT-5/ATP9A, NDK-1/NME1, and APC-2/ANAPC2 are required for the integrity of the migrating male nematode gonad

We assayed the mutant worms for a linker cell detachment phenotype to test whether worm orthologs of the candidate genes are also required for cell adhesion. During the development of the nematode male, the linker cell leads a collective migratory process that shapes the male gonad and connects the gonadal lumen to the cloaca, opening up the passage for sperm (Kimble and Hirsh, 1979; Sulston et al., 1980). Disruption of this process, including the detachment of the linker cell, thus resulted in the male gonad not being connected to the exterior. We find that similar to that of *lnkn-1(lf)*, high occurrences of nonconnected gonads were observed in male animals carrying the mutation alleles of *tat-5*, *ndk-1*, *apc-2*, and *lin-40* (Fig. 6A).

To determine whether the enclosed gonads were the results of linker cell detachment, we examined the gonads of developing animals. We found that as with that of *lnkn-1(lf)* (Fig. 6B), detached linker cells (LC) were observed in animals carrying the mutation alleles of *tat-5* (Fig. 6C)*, ndk-1* (Fig. 6D), and *apc-2* (Fig. 6E). The phenotype, however, was rarely observed in *lin-40(lf)*. Instead, the defect in *lin-40(lf)* animals seems to be caused by a late-stage pathfinding defect. Nonetheless, our results found that the worm orthologs of ATP9A, NME1, NME4, and ANAPC2 were essential for a physiological process that relies heavily on cell adhesiveness. This and the fact that LNKN-1 is known to be critical for the same process give further credence to both their ITFG1 association and the role of LINKIN in cell adhesion.

Discussion

By combining proteomics and association studies in cultured human cells with genetic analysis in C. elegans, we have identified four proteins that both are physically associated with LINKIN and play roles in the same process. This concordance of physical and genetic interaction places them firmly in the same cellular sub-network.

Linker cell migration as a discovery platform for regulators of collective migration and adhesion

Since its establishment as a genetic model (Brenner, 1974), *C. elegans* has been among the favorite of developmental biologists. Among the useful features it offers are its

simplicity, invariant development, and a largely transparent body (Corsi et al., 2015). The collective migration of the male gonad led by the linker cell offers an excellent example of such. Starting in the L2 larvae stage, the linker cell migrated along a complicated trajectory that involves multiple turns, each occurring at a precise timing coordinating with the development of the animal, reaching the cloaca during L4 and underwent programmed cell death, opening up the sperm passage (Abraham et al., 2007; Hedgecock et al., 1987; Kato and Sternberg, 2009; Kimble and Hirsh, 1979). The entire process can be followed under microscopy, and the shape of the gonad can also be seen as a record of the path taken by the linker cell. While much more attention has been focused on the shaping of the hermaphroditic gonads, linker cells have been studied from a few different perspectives. First of all, it has been utilized as a model to study cell migration, often in conjunction with the study of other cell types, such as the axon migration in neurons and, in particular, the distal tip cell of the hermaphrodites (Antebi et al., 1998; Blelloch et al., 1999; Blelloch and Kimble, 1999; Clark et al., 1993; Hedgecock et al., 1990; Hedgecock et al., 1987; Kato et al., 2021; Kato and Sternberg, 2009; Nishiwaki, 1999; Nishiwaki et al., 2000; Palmer et al., 2002; Su et al., 2000; Tamai and Nishiwaki, 2007; Vogel and Hedgecock, 2001). The LC undergoes a caspase-independent form of programmed cell death (Abraham et al., 2007; Blum et al., 2012; Denning et al., 2013; Keil et al., 2017; Kinet et al., 2016; Lee et al., 2019; Malin et al., 2016; Schwendeman and Shaham, 2016). As part of the effort to understand its biology, the transcriptome of the cell, acquired through physical isolation, is known at different stages during its development (Schwarz et al., 2012). Finally, related to this study, linker cell has been studied in relation to cell adhesion (Kato et al., 2014).

In *C. elegans*, the male gonad development offers a unique opportunity to study postembryonic collective cell migration. While sharing many aspects in their development, particularly the migratory orientations, the Linker cell lead collective migration of the male gonad is mechanically very different from the distal tip cell-oriented gonad shaping in hermaphrodites. The linker cell unequivocally moves itself forward, as seen both in mutants with the cells detached and those physically cut off from the rest of the gonad (Chisholm, 1991; Kato et al., 2014; Sternberg and Horvitz, 1988). In either case, the linker cell continues its normal course of migration. Here, we argue that, as we present in this

study and that in Kato et al. (2014), linker cell migration is also a great genetic model for cell adhesion research, in particular, cell adhesion during migration. We reasoned that the reason that linker cell detachment happens in homozygous mutant animals descended from heterozygotic mothers that were otherwise viable is due to 1) The encoded protein was provided maternally earlier in the development, where most other collective migrations occur. 2) The probable intense stress applied to the cells from the tow. Coupled these with a distinctive visible phenotype, we proposed it as an excellent platform for future discovery.

A diverse group of proteins is required to keep the migrating cells together.

Mutant animals of three orthologs of four ITFG1 interactors were found to have the linker cell detachment phenotype. The phenotype, likely associated with cell adhesion, is also found in the mutant animals of *lnkn-1*, the worm ortholog of ITFG1. Animals carrying the mutant alleles of the three orthologs *tat-5*/ATP9A, *ndk-1*/NME1/4, and *apc-2*/ANAPC2, also displayed other phenotypes that we observed in *lnkn-1(lf)* animals, suggesting evolvement in similar biological process.

tat-5, orthologs of the mammalian ATP9A and ATP9B belong to the eukaryotic P4-type ATPases family of proteins (Lyssenko et al., 2008). These ATPase (flippase) actively transport phospholipids between the two leaflets of the membrane (Andersen et al., 2016). The worm genome encodes six members of the family, of which *tat-5* is the only one that is essential (Lyssenko et al., 2008). Previous studies suggest that TAT-5 maintains phosphatidylethanolamine (PE) asymmetry in the membrane and suppresses the budding of extracellular vesicles, and loss of *tat-5* results in abnormal embryonic cell shape, which may be due to reduced cell adhesion (Beer et al., 2018; Wehman et al., 2011).

NDK-1 is the sole group I member of the NME proteins in *C. elegans* (Masoudi et al., 2013). Also known as NM23 (non-metastatic 23) / NDPK nucleoside diphosphate kinase, the family is broadly conserved in evolution (Bilitou et al., 2009; Cetkovic et al., 2015). The first member of the family, a group I member, NME1, was the first identified

metastasis suppressor gene (Steeg et al., 1988). Two group I NME proteins- NME1 and NME 4 were enriched in both of the ITFG1-pulldown assays (Table S1-3). Studies of the group in cell lines and model organisms suggest its involvement in developmental processes, including migration and cell proliferation (Matyasi et al., 2020). Notably, NME1 is argued to locally produce GTP for use by GTPases such as dynamin (Farkas et al., 2019). Previous studies of NDK-1 in *C. elegans* suggest its involvement in the Ras/MAPK signaling, apoptosis, and the shaping of the hermaphroditic gonad (Fancsalszky et al., 2014; Farkas et al., 2018; Farkas et al., 2019; Masoudi et al., 2013; Tran et al., 2019).

apc-2 encodes the worm ortholog of human ANAPC2 (anaphase promoting complex subunit 2). The anaphase promoting complex (APC), also known as cyclosome, is an E3 ubiquitin ligase that is essential for the progression of eukaryotic cell cycles (Peters, 2006). It is thought that the activities of APC can affect gene expression, at least at the chromatin level (Bodrug et al., 2021).

How might these three very different proteins be involved in holding the migrating cells together? Kato et al. (2014) suggest that LNKN-1, with its extracellular domain containing motifs with similarities to that of integrin, is likely to be directly involved in physical adhesion. Based on that model, the intracellular domain of LNKN-1 interacts with RUVB-1, RUVB-2, and alpha-tubulin, connecting the junction to the microtubule cytoskeleton. The model was supported through protein interactions of their human counterpart in cultured cells, which we again validated in this study, and of colocalization in the worm gonad. Previous studies find the TAT-5 to be associated with cell adhesion (Wehman et al., 2011), presumably depending on its flippase activity. It is possible that LNKN-1 and TAT-5 are closely associated at the adhesion junction and reinforce an adhesive environment. As a nucleoside diphosphate kinase, it is plausible that NDK-1 is recruited by LNKN-1 or its associated protein for its enzymatic properties, perhaps for a yet to be identified G protein that functions locally to promote cell adhesion. Based on the cell detachment phenotype, a few other proteins were also identified, although it is not known whether they are directly involved since no interaction was found between their orthologs and that of ITFG1. Those proteins include EGL-5 (Chisholm, 1991; Schwarz et al., 2012), which, as a homeobox transcription factor, is likely to be indirectly involved. Other proteins

are orthologs of each of the SMC (Structural maintenance of chromosomes) proteins 1-4 (Schwarz et al., 2012), which are the core parts of the cohesin and condensin complexes (Hirano, 2006). The addition of a component of the anaphase promoting complex, APC-2, raises the question of why the LINKIN interactome includes significant number of chromosomes associated proteins. A default explanation is that this is due to an indirect effect of cell cycle events on the post-mitotic linker cell. Another hypothesis is that chromosome biology plays a structural role. An intriguing review by (Bustin and Misteli, 2016)) argues that chromosomes, as large entities in the cell, have other roles in cell processes unrelated to genome integrity and gene expression. We propose that the linker cell chromosomes help anchor the cytoskeleton and membrane adhesion molecules, making the nucleus a huge anchor that can withstand the force of collective cell migration.

Materials and Methods

Knowledgebases

We used WormBase (Davis et al., 2022), the Alliance of Genome Resources (Alliance of Genome Resources, 2022), STRING (Szklarczyk et al., 2023), GeneMania (Franz et al., 2018) in the design and interpretation of experiments.

Plasmid construction and cell lines

The full-length ITFG1 with or without a C-terminal Myc tag (OriGene Technologies, Inc., RC204773) was cloned in the expression vector pcDNA3.3 or pRRL.sin.cPPT.SFFV/IRES-neo.WPRE. The full-length RUVBL1 with N-terminal 3×FLAG tag (pCDNA-3xFLAG-Pontin) was obtained from Addgene (51635). All cell lines were grown in DMEM (Sigma-Aldrich) supplemented with 10% fetal bovine serum (FBS, Atlanta Biologicals) plus 100 U/mL penicillin and 100 µg/mL streptomycin (Lonza) and maintained at 37°C with 5% CO_2. Transfection was performed using BioT (Bioland Scientific LLC). MDA-MB-231 cells were transiently transfected with pcDNA3.3 expressing ITFG1-Myc or ITFG1. MDA-MB-231 stably expressing ITFG1-Myc were generated by transduction with pseudotyped lentiviral vector produced by transient co-transfection of 293T cells with pRRL.sin.cPPT.SFFV/IRES-neo.WPRE expressing ITFG-

Myc plasmid and lentivirus packaging plasmids (pHDM-G, CAG4-RTR2 and CAGGHIVgpco). Stable cell lines were selected in the presence of 5 mg/mL G418 24 h post-lentivirus infection. MDA-MB-231 cells stably expressing ITFG1-Myc were transfected with pCDNA-3xFLAG-Pontin for transient expression of FLAG-RUVBL1.

RNA extraction and qPCR analysis

Total cell RNA was extracted from cells using the MagMAX *mir*Vana Total RNA Isolation Kit (Applied Biosystems, A27828) with KingFisher Duo Prime Purification System (Thermo Scientific). We converted total RNA to cDNA using High-Capacity cDNA Reverse Transcription Kit (Applied Biosystems, 4368813). Quantitative PCR (qPCR) was performed on the QuantStudio™ 5 Real-Time PCR System (Applied Biosystems) using PowerUp SYBR Green Master Mix (Applied Biosystems, A25741). Primer sequences of ITFG1 used in qPCR: TGGGAGCTGACAGACCTAAA and GCAGTAAGCAGAACAATATTACTTGG. ITFG1 RNA level was normalized to GAPDH as a reference gene.

Western blot assay

Protein samples from cell lysate or immunoprecipitation elution were loaded on 4-20% SDS-PAGE gel (Bio-Rad) and transferred to a nitrocellulose membrane (Bio-Rad). The following primary antibodies were used for protein blotting: mouse anti-c-Myc antibody (Sigma-Aldrich, 05-724MG), mouse anti-Flag antibody (Sigma-Aldrich, F3165), Rabbit anti-ITFG1 antibody (ITFG1_Ab1) (Invitrogen, PA5-54067), mouse anti-ITFG1 antibody (ITFG1_Ab2) (R&D Systems, MAB89001), Rabbit anti-RUVBL1 antibody (Proteintech, 10210-2-AP), Rabbit anti-GAPDH antibody (Cell Signaling Technology, 2118). Signals were developed with HRP-labeled secondary antibodies (Bio-Rad). Blots were developed using Immobilon Western Chemiluminescent HRP Substrate (Millipore) and visualized using ChemiDoc MP Imaging System (Bio-Rad).

Immunofluorescence staining

Cells were seeded in a 96-well plate, which was coated with 20 mg/mL fibronectin (Sigma-Aldrich, F1141). On the next day, cells were fixed in ice-cold 4% paraformaldehyde at room temperature for 5 min. After blocking with 10% FBS plus 0.2% Triton X-100 at room temperature for 1 h, cells were overnight incubated with Rabbit anti-ITFG1 antibody (Invitrogen, PA5-54067) at 4°C, followed by Alexa FluorTm 594 donkey anti-rabbit IgG (H+L) (Invitrogen, A21207) at room temperature for 1.5 h. Cells were counter stained with Hoechst 33342 (Thermo Scientific, 62249) and visualized with an ImageXpress® Confocal HT.ai High-Content Imaging System (Molecular Devices).

Flow cytometry

Surface expression of ITFG1 on cells was examined by staining the cells with mouse anti-ITFG1 antibody (R&D Systems, MAB89001) at 4°C for 1 hour, followed by Alexa Fluor 488 donkey anti-mouse IgG (H+L) (Invitrogen, A21202). The surface florescence intensity of viable cells was measured by S3e Cell Sorter (Bio-Rad).

In-gel digestion

Cell lysates from ITFG1-FL-Myc-expressing MDA-MB-231 and MDA-MB-231 cells were separated in a 4-20% SDS-PAGE gel (Bio-Rad). The gels were stained with Imperial Protein Stain (Thermo Scientific, 24615). Gel lanes in the molecular weight range between 150 and 250 kDa, 75 and 150 kDa , and 37 and 75 kDa were removed and further excised into small pieces 1.5 ml tube followed by in-gel digested using Tryptic Digestion Kit (Thermo Scientific, 89871) according to the manufacturer's instructions. After digestion, digested mixtures were dried using vacuum centrifugation and dissolved with 0.1% formic acid for LC-MS/MS analysis.

Immunoprecipitation and sample preparation for LC-MS/MS

Each immunoprecipitation was performed in triplicate. Cell lysates were prepared in lysis buffer (20 mM HEPES pH 7.5, 100 mM NaCl, 0.2% n-dodeyl-D-Maltoside, 1 mM N-Ethylmaleimide, 1% Triton-100, 0.02 mM MG132, and Pierce protease inhibitors (Thermo Scientific, A32965). Protein concentration was determined using the Bradford protein assay (Bio-Rad). Equivalent amounts of protein (~2 mg) were used for immunoprecipitation with Pierce anti-c-Myc Agarose (Thermo Scientific, 20169), anti-Flag

Affinity Gel (Bimake, B23101), or anti-ITFG1 antibody-conjugated agarose. Two anti-ITFG1 antibodies were covalently conjugated on agarose beads using Pierce Direct IP Kit (Thermo Scientific, 26148), respectively. Immunoprecipitation was performed at 4°C for 2 h in micro-spin column (Thermo Scientific, 89879), and the beads were washed three times with lysis buffer and two times with Mass Spec buffer (0.1 M Tris-HCl in mass grade water, pH 8.5). Proteins were eluted with 10 M urea solution and prepared for LC-MS/MS analysis using EasyPep Mini MS Sample Prep Kit (Thermo Scientific, A40006). The dried peptides were dissolved with 0.1% formic acid.

LC-MS/MS and protein identification

LC-MS/MS experiments were performed using EASY-nLC1000 (Thermo Fisher Scientific) connected to an Orbitrap Eclipse Tribrid mass spectrometer (Thermo Fisher Scientific). The detailed information for LC/MS processing and data analysis was described previously (Cheng et al., 2021). System control and data collection were performed by Xcalibur v.4.0. Proteomic analysis was performed with the Proteome Discoverer 2.4 (Thermo Scientific) using the SequestHT search algorithm with Percolator validation. A set of proteins = upregulated in ITFG-Myc-expressing cells compared to non-expressing control cells in at least two immunoprecipitates were identified (log2 FC > 0.6), in which proteins with higher upregulated (log2 FC > 2) were selected for overlap analysis. Venn plots were generated with FunRich 3.1.4 (Fonseka et al., 2021; Pathan et al., 2015; Pathan et al., 2017). The resulting list of overlapped proteins was subjected to Reactome pathway and Gene Ontology (GO) biological process enrichment analysis using Metascape(Zhou et al., 2019)

Nematode genetics and general methods

The strains of *C. elegans* were maintained using standard methods similar to what was described by Brenner (1974). Briefly, worms were cultured on Nematode Growth Medium (NGM) dishes seeded with a lawn of Escherichia coli strain OP50 at 20°C. All strains were derived from the wild-type reference strain Bristol N2 (Brenner, 1974). Alleles and transgenes used in this study were: LG I: *src-1(cj293)* (Bei et al., 2002), *dpy-5(e61), unc-13(e450)* (Brenner, 1974), *unc-94(ok1210), cdc-25.1(ok1888), ndk-1(ok314)* (Consortium, 2012), *feh-1(gb561)* (Zambrano et al., 2002), *tat-5(tm1741)*, *tmC18[dpy-5(tmIs1200)]*,

tmC18[dpy-5(tmIs1236)], tmC27[unc-75(tmIs1239)] (Dejima et al., 2018), *let-611(h826)*; LG II: *syIs128* (Kato and Sternberg, 2009); LG III: *apc-2(ok1657)* (Consortium, 2012), *oxTi719*, *oxTi956* (Frokjaer-Jensen et al., 2014), *lnkn-1(sy1596), mvk-1(tm6628), trd-1(tm2764), qC1 [dpy-19(e1259) glp-1(q339)] nIs189, sC1(s2023)[dpy-1(s2170)umnIs21]*; LG IV: *him-8 (Hodgkin et al., 1979), rad-51(ok2218)* (Consortium, 2012), *rod-1(tm6186), tmC5[F36H1.3(tmIs1220)]* (Dejima et al., 2018); LG V: *him-5 (Hodgkin et al., 1979)*, *cdc-25.2(ok597), C10B5.1(ok3270), hsp-90(ok1333), lin-40(gk255), lin-40(ok905), lin-40(ok906)* (Consortium, 2012), *tmC3[egl-9(tmIs1228)], tmC3[egl-9(tmIs1230)], tmC12[egl-9(tmIs1197)], tmC16[unc-60(tmIs1210)], tmC16[unc-60(tmIs1237)]* (Dejima et al., 2018); LG X: *vps-41(ok3433)* (Consortium, 2012), *tmC30[ubc-17(tmIs1243)], tmC30[ubc-17(tmIs1247)]* (Dejima et al., 2018).

Generation of *lnkn-1(sy1596)* loss-of-function allele

The *lnkn-1(sy1596)* knock-out animal was generated by CRISPR/Cas9, using the STOP-IN cassette strategy as described in Wang et al. (2018). The 43bp knock-in cassette (GGGAAGTTTGTCCAGAGCAGAGGTGACTAAGTGATAAgctagc) was inserted near the 5' end of the coding region between CTTGGAAAAGTATGTGCATTTGGAGATTTCAATGCA and GATCGGAATACTGATATTCTGGTTTTTGCGAATG. The *lnkn-1(sy1593)* (III:-0.01) mutation was maintained *in trans* by two inserted fluorescent marker *oxTi719[eft-3p::tdTomato::H2B]* (III:-0.26) and *oxTi956[eft-3p::GFP::2xNLS::tbb-2]* (III: 0.03) (Frokjaer-Jensen et al., 2014).

Balancer strain construction

We obtained alleles for candidate genes based on: (1) The existence of an available allele; (2) A judgmental call based on available information from Worm Base https://wormbase.org (Davis et al., 2022); Caenorhabditis Genetics Center https://cgc.umn.edu; and in NBRP of Japan https://nbrp.jp/en/resource/c-elegans-en, in whether the allele was described as either lethal or sterile; (3) Whether the allele was available without other mutations in *cis*. We then rebalanced many of the obtained alleles with balancers (Dejima et al., 2018) that are intrachromosomal and fluorescently labeled (Table S6).

Microscopy

Images were acquired with a Zeiss Imager Z2 microscope equipped with an Apotome 2 and Axiocam 506 mono using Zen 2 Blue software. Worms were immobilized with levamisole and mounted on 5% agarose pads on microscope slides for observation.

Development and fertility assay of hermaphrodite worms

All homozygous hermaphrodites of the lethal or sterile mutations used in this study descended from balanced heterozygotic mothers. homozygous animals were identified through the lack of fluorescently labeled balancers. In Fig. 4C, mutations that prevented worms from adulthood were excluded from further analysis. Phenotype 2 was defined by having F_1 progenies that hatch. Phenotype 3 was defined by the observation of embryos/ embryo-like objects or oocytes on the NGM plates in which the worm was cultured. Some worms that very rarely (*unc-94*) or never (like *rod-1*) lay anything were observed to possess embryos and oocytes inside the gonad. In the maternal effect experiments (Fig. 4B-C phenotype 4,5), homozygous hermaphrodites were mated with *him-5(e1490)* males carrying fluorescent genetic markers *oxTi719* [*eft-3p::tdTomato::H2B*] and *oxTi956[eft-3p::GFP::2xNLS::tbb-2]*. Due to large differences in brightness, only *oxTi719* was assayed for the experiment. Phenotype 4 was determined by whether the male-derived *oxTi719* marker was observed in F1 embryos/animals, as seen in Fig. 4B-Phenotype 5 was based on whether those F1 (as in phenotype 4) hatch.

Assessment and measurement of the gonad phenotype in hermaphrodites.

The measurement and analysis of the gonad phenotype in hermaphrodites were performed as described in Fig. 5C. The measurement was done using the ImageJ software (NIH) with homozygous hermaphrodites two days past L4. The approximated ventral-proximal gonad arm lengths were measured by drawing a line through the midline of the worm as the distance from the vulval to the ventral-dorsal turn of the U-shaped gonad arm. The approximated dorsal-distal gonad arm lengths were measured similarly, as the distance from the distal end of the gonad to the ventral-dorsal turn. The Centripetal migration (%) was calculated by dividing the value of dorsal-distal gonad arm length by the value of ventral-proximal gonad arm length and multiplying by 100%. Due to the

positioning of the worms on the microscope slide, not all worms were measured for both arms of the gonad. Pathfinding or other gonadal development defects were observed in some of the mutants, and animals exhibiting those phenotypes were not included in this examination. All comparison in Fig. 5D was to the value of the wild-type, using two-tailed, unpaired Student's *t*-test.

Assessment of male gonad development and linker cell migration analysis

For Fig. 6, all homozygous males descended from balanced heterozygotic mothers, and all carry the transgene *syIs128 [lag-2p::YFP]* (Kato and Sternberg, 2009), which labels the cytoplasm of the linker cell. In addition, all strains carry either *him-5(e1490)* or *him-8(e1489)* (Hodgkin et al., 1979) to increase male occurrence. The male *apc-2(ok1657)* homozygous males have other clear tail morphological defects post-L4, but the linker cell detachment precedes that development. In Fig.6B-E, the linker cell was identified through both the cell morphology under DIC and the transgene *syIs128.*

Acknowledgements

We thank Barbara Perry, Wilber Palma and Stephanie Nava for laboratory assistance. We thank members of our laboratory for discussions. Mutant alleles- *mvk-1(tm6628)*, *trd-1(tm2764), vha-19(tm2225), prx-3(tm6469),* and *rod-1(tm6186)* were provided by the MITANI Lab through the National Bio-Resource Project of the MEXT, Japan. Some strains were obtained from the Caenorhabditis Genetics Center (CGC), which is funded by the NIH Office of Research Infrastructure Programs (P40 OD010440). This work was also facilitated by WormBase, a knowledgebase for nematode research; and by the Alliance of Genome Resources, a research platform that facilitates cross species research, This research was supported by NIH R01HD086596 (PWS and TFC), R01HD091327 (PWS), and R24 0D023041 (PWS).

References

Abraham, M. C., Lu, Y. and Shaham, S. (2007). A morphologically conserved nonapoptotic program promotes linker cell death in Caenorhabditis elegans. *Developmental cell* **12**, 73-86.

Agarwal, P., Shemesh, T. and Zaidel-Bar, R. (2022). Directed cell invasion and asymmetric adhesion drive tissue elongation and turning in C. elegans gonad morphogenesis. *Developmental cell* **57**, 2111-2126 e2116.

Alliance of Genome Resources, C. (2022). Harmonizing model organism data in the Alliance of Genome Resources. *Genetics* **220**.

Andersen, J. P., Vestergaard, A. L., Mikkelsen, S. A., Mogensen, L. S., Chalat, M. and Molday, R. S. (2016). P4-ATPases as Phospholipid Flippases-Structure, Function, and Enigmas. *Front Physiol* **7**, 275.

Antebi, A., Culotti, J. G. and Hedgecock, E. M. (1998). daf-12 regulates developmental age and the dauer alternative in Caenorhabditis elegans. *Development* **125**, 1191-1205.

Ashcroft, N. and Golden, A. (2002). CDC-25.1 regulates germline proliferation in Caenorhabditis elegans. *Genesis* **33**, 1-7.

Beer, K. B., Rivas-Castillo, J., Kuhn, K., Fazeli, G., Karmann, B., Nance, J. F., Stigloher, C. and Wehman, A. M. (2018). Extracellular vesicle budding is inhibited by redundant regulators of TAT-5 flippase localization and phospholipid asymmetry. *Proceedings of the National Academy of Sciences of the United States of America* **115**, E1127-E1136.

Bei, Y., Hogan, J., Berkowitz, L. A., Soto, M., Rocheleau, C. E., Pang, K. M., Collins, J. and Mello, C. C. (2002). SRC-1 and Wnt signaling act together to specify endoderm and to control cleavage orientation in early C. elegans embryos. *Developmental cell* **3**, 113-125.

Bilitou, A., Watson, J., Gartner, A. and Ohnuma, S. (2009). The NM23 family in development. *Mol Cell Biochem* **329**, 17-33.

Blelloch, R., Anna-Arriola, S. S., Gao, D., Li, Y., Hodgkin, J. and Kimble, J. (1999). The gon-1 gene is required for gonadal morphogenesis in Caenorhabditis elegans. *Developmental biology* **216**, 382-393.

Blelloch, R. and Kimble, J. (1999). Control of organ shape by a secreted metalloprotease in the nematode Caenorhabditis elegans. *Nature* **399**, 586-590.

Blum, E. S., Abraham, M. C., Yoshimura, S., Lu, Y. and Shaham, S. (2012). Control of nonapoptotic developmental cell death in Caenorhabditis elegans by a polyglutamine-repeat protein. *Science* **335**, 970-973.

Bodrug, T., Welsh, K. A., Hinkle, M., Emanuele, M. J. and Brown, N. G. (2021). Intricate Regulatory Mechanisms of the Anaphase-Promoting Complex/Cyclosome and Its Role in Chromatin Regulation. *Front Cell Dev Biol* **9**, 687515.

Brenner, S. (1974). The genetics of Caenorhabditis elegans. *Genetics* **77**, 71-94.

Bustin, M. and Misteli, T. (2016). Nongenetic functions of the genome. *Science* **352**, aad6933.

Cetkovic, H., Perina, D., Harcet, M., Mikoc, A. and Herak Bosnar, M. (2015). Nme family of proteins--clues from simple animals. *Naunyn Schmiedebergs Arch Pharmacol* **388**, 133-142.

Cheng, K. W., Li, S., Wang, F., Ruiz-Lopez, N. M., Houerbi, N. and Chou, T. F. (2021). Impacts of p97 on Proteome Changes in Human Cells during Coronaviral Replication. *Cells* **10**.

Chisholm, A. (1991). Control of cell fate in the tail region of C. elegans by the gene egl-5. *Development* **111**, 921-932.

Clark, S. G., Chisholm, A. D. and Horvitz, H. R. (1993). Control of cell fates in the central body region of C. elegans by the homeobox gene lin-39. *Cell* **74**, 43-55.

Collins, C. and Nelson, W. J. (2015). Running with neighbors: coordinating cell migration and cell-cell adhesion. *Current opinion in cell biology* **36**, 62-70.

Consortium, C. e. D. M. (2012). large-scale screening for targeted knockouts in the Caenorhabditis elegans genome. *G3* **2**, 1415-1425.

Corsi, A. K., Wightman, B. and Chalfie, M. (2015). A Transparent Window into Biology: A Primer on Caenorhabditis elegans. *Genetics* **200**, 387-407.

Cram, E. J., Shang, H. and Schwarzbauer, J. E. (2006). A systematic RNA interference screen reveals a cell migration gene network in C. elegans. *Journal of cell science* **119**, 4811-4818.

Davis, P., Zarowiecki, M., Arnaboldi, V., Becerra, A., Cain, S., Chan, J., Chen, W. J., Cho, J., da Veiga Beltrame, E., Diamantakis, S., et al. (2022). WormBase in 2022-data, processes, and tools for analyzing Caenorhabditis elegans. *Genetics*.

Dejima, K., Hori, S., Iwata, S., Suehiro, Y., Yoshina, S., Motohashi, T. and Mitani, S. (2018). An Aneuploidy-Free and Structurally Defined Balancer Chromosome Toolkit for Caenorhabditis elegans. *Cell reports* **22**, 232-241.

Denning, D. P., Hatch, V. and Horvitz, H. R. (2013). Both the caspase CSP-1 and a caspase-independent pathway promote programmed cell death in parallel to the canonical pathway for apoptosis in Caenorhabditis elegans. *PLoS genetics* **9**, e1003341.

Evans, T. C. and Hunter, C. P. (2005). Translational control of maternal RNAs. *WormBook : the online review of C. elegans biology*, 1-11.

Fan, W., Xie, J., Xia, J., Zhang, Y., Yang, M., Wang, H., Pan, Y., Zhang, M., Han, B., Wu, B., et al. (2017). RUVBL1-ITFG1 interaction is required for collective invasion in breast cancer. *Biochim Biophys Acta Gen Subj* **1861**, 1788-1800.

Fancsalszky, L., Monostori, E., Farkas, Z., Pourkarimi, E., Masoudi, N., Hargitai, B., Bosnar, M. H., Dezeljin, M., Zsakai, A., Vellai, T., et al. (2014). NDK-1, the homolog of NM23-H1/H2 regulates cell migration and apoptotic engulfment in C. elegans. *PloS one* **9**, e92687.

Farkas, Z., Fancsalszky, L., Saskoi, E., Graf, A., Tarnok, K., Mehta, A. and Takacs-Vellai, K. (2018). The dosage-dependent effect exerted by the NM23-H1/H2 homolog NDK-1 on distal tip cell migration in C. elegans. *Lab Invest* **98**, 182-189.

Farkas, Z., Petric, M., Liu, X., Herit, F., Rajnavolgyi, E., Szondy, Z., Budai, Z., Orban, T. I., Sandor, S., Mehta, A., et al. (2019). The nucleoside diphosphate kinase NDK-1/NME1 promotes phagocytosis in concert with DYN-1/Dynamin. *FASEB journal : official publication of the Federation of American Societies for Experimental Biology* **33**, 11606-11614.

Felix, M. A. and Sternberg, P. W. (1996). Symmetry breakage in the development of one-armed gonads in nematodes. *Development* **122**, 2129-2142.

Fonseka, P., Pathan, M., Chitti, S. V., Kang, T. and Mathivanan, S. (2021). FunRich enables enrichment analysis of OMICs datasets. *Journal of molecular biology* **433**, 166747.

Franz, M., Rodriguez, H., Lopes, C., Zuberi, K., Montojo, J., Bader, G. D. and Morris, Q. (2018). GeneMANIA update 2018. *Nucleic acids research* **46**, W60-W64.

Frokjaer-Jensen, C., Davis, M. W., Sarov, M., Taylor, J., Flibotte, S., LaBella, M., Pozniakovsky, A., Moerman, D. G. and Jorgensen, E. M. (2014). Random and targeted transgene insertion in Caenorhabditis elegans using a modified Mos1 transposon. *Nature methods* **11**, 529-534.

Geiger, T. R. and Peeper, D. S. (2009). Metastasis mechanisms. *Biochimica et biophysica acta* **1796**, 293-308.

Greenwald, I. S., Sternberg, P. W. and Horvitz, H. R. (1983). The lin-12 locus specifies cell fates in Caenorhabditis elegans. *Cell* **34**, 435-444.

Hedgecock, E. M., Culotti, J. G. and Hall, D. H. (1990). The unc-5, unc-6, and unc-40 genes guide circumferential migrations of pioneer axons and mesodermal cells on the epidermis in C. elegans. *Neuron* **4**, 61-85.

Hedgecock, E. M., Culotti, J. G., Hall, D. H. and Stern, B. D. (1987). Genetics of cell and axon migrations in Caenorhabditis elegans. *Development* **100**, 365-382.

Hirano, T. (2006). At the heart of the chromosome: SMC proteins in action. *Nat Rev Mol Cell Biol* **7**, 311-322.

Hirsh, D., Oppenheim, D. and Klass, M. (1976). Development of the reproductive system of Caenorhabditis elegans. *Developmental biology* **49**, 200-219.

Hodgkin, J., Horvitz, H. R. and Brenner, S. (1979). Nondisjunction Mutants of the Nematode CAENORHABDITIS ELEGANS. *Genetics* **91**, 67-94.

Hughes, S., Wilkinson, H., Gilbert, S. P., Kishida, M., Ding, S. S. and Woollard, A. (2014). The C. elegans TPR Containing Protein, TRD-1, Regulates Cell Fate Choice in the Developing Germ Line and Epidermis. *PloS one* **9**, e114998.

Hunt-Newbury, R., Viveiros, R., Johnsen, R., Mah, A., Anastas, D., Fang, L., Halfnight, E., Lee, D., Lin, J., Lorch, A., et al. (2007). High-throughput in vivo analysis of gene expression in Caenorhabditis elegans. *PLoS biology* **5**, e237.

Hynes, R. O. (1999). Cell adhesion: old and new questions. *Trends Cell Biol* **9**, M33-37.

Janiszewska, M., Primi, M. C. and Izard, T. (2020). Cell adhesion in cancer: Beyond the migration of single cells. *The Journal of biological chemistry* **295**, 2495-2505.

Kato, M., Chou, T. F., Yu, C. Z., DeModena, J. and Sternberg, P. W. (2014). LINKIN, a new transmembrane protein necessary for cell adhesion. *eLife* **3**, e04449.

Kato, M., Kolotuev, I., Cunha, A., Gharib, S. and Sternberg, P. W. (2021). Extrasynaptic acetylcholine signaling through a muscarinic receptor regulates cell migration. *Proceedings of the National Academy of Sciences of the United States of America* **118**.

Kato, M. and Sternberg, P. W. (2009). The C. elegans tailless/Tlx homolog nhr-67 regulates a stage-specific program of linker cell migration in male gonadogenesis. *Development* **136**, 3907-3915.

Keil, W., Kutscher, L. M., Shaham, S. and Siggia, E. D. (2017). Long-Term High-Resolution Imaging of Developing C. elegans Larvae with Microfluidics. *Developmental cell* **40**, 202-214.

Kim, J., Kawasaki, I. and Shim, Y. H. (2010). cdc-25.2, a C. elegans ortholog of cdc25, is required to promote oocyte maturation. *Journal of cell science* **123**, 993-1000.

Kim, J., Lee, A. R., Kawasaki, I., Strome, S. and Shim, Y. H. (2009). A mutation of cdc-25.1 causes defects in germ cells but not in somatic tissues in C. elegans. *Mol Cells* **28**, 43-48.

Kimble, J. (1981). Alterations in cell lineage following laser ablation of cells in the somatic gonad of Caenorhabditis elegans. *Developmental biology* **87**, 286-300.

Kimble, J. and Hirsh, D. (1979). The postembryonic cell lineages of the hermaphrodite and male gonads in Caenorhabditis elegans. *Developmental biology* **70**, 396-417.

Kimble, J. E. and White, J. G. (1981). On the control of germ cell development in Caenorhabditis elegans. *Developmental biology* **81**, 208-219.

Kinet, M. J., Malin, J. A., Abraham, M. C., Blum, E. S., Silverman, M. R., Lu, Y. and Shaham, S. (2016). HSF-1 activates the ubiquitin proteasome system to promote non-apoptotic developmental cell death in C. elegans. *eLife* **5**.

Klass, M., Wolf, N. and Hirsh, D. (1976). Development of the male reproductive system and sexual transformation in the nematode Caenorhabditis elegans. *Developmental biology* **52**, 1-18.

Lee, Y., Hamann, J. C., Pellegrino, M., Durgan, J., Domart, M. C., Collinson, L. M., Haynes, C. M., Florey, O. and Overholtzer, M. (2019). Entosis Controls a Developmental Cell Clearance in C. elegans. *Cell reports* **26**, 3212-3220 e3214.

Lyssenko, N. N., Miteva, Y., Gilroy, S., Hanna-Rose, W. and Schlegel, R. A. (2008). An unexpectedly high degree of specialization and a widespread involvement in sterol metabolism among the C. elegans putative aminophospholipid translocases. *BMC developmental biology* **8**, 96.

Malin, J. A., Kinet, M. J., Abraham, M. C., Blum, E. S. and Shaham, S. (2016). Transcriptional control of non-apoptotic developmental cell death in C. elegans. *Cell Death Differ* **23**, 1985-1994.

Masoudi, N., Fancsalszky, L., Pourkarimi, E., Vellai, T., Alexa, A., Remenyi, A., Gartner, A., Mehta, A. and Takacs-Vellai, K. (2013). The NM23-H1/H2 homolog NDK-1 is required for full activation of Ras signaling in C. elegans. *Development* **140**, 3486-3495.

Matyasi, B., Farkas, Z., Kopper, L., Sebestyen, A., Boissan, M., Mehta, A. and Takacs-Vellai, K. (2020). The Function of NM23-H1/NME1 and Its Homologs in Major Processes Linked to Metastasis. *Pathol Oncol Res* **26**, 49-61.

Mayor, R. and Etienne-Manneville, S. (2016). The front and rear of collective cell migration. *Nat Rev Mol Cell Biol* **17**, 97-109.

Miwa, J., Schierenberg, E., Miwa, S. and von Ehrenstein, G. (1980). Genetics and mode of expression of temperature-sensitive mutations arresting embryonic development in Caenorhabditis elegans. *Developmental biology* **76**, 160-174.

Nishiwaki, K. (1999). Mutations affecting symmetrical migration of distal tip cells in Caenorhabditis elegans. *Genetics* **152**, 985-997.

Nishiwaki, K., Hisamoto, N. and Matsumoto, K. (2000). A metalloprotease disintegrin that controls cell migration in Caenorhabditis elegans. *Science* **288**, 2205-2208.

Palmer, R. E., Inoue, T., Sherwood, D. R., Jiang, L. I. and Sternberg, P. W. (2002). Caenorhabditis elegans cog-1 locus encodes GTX/Nkx6.1 homeodomain proteins and regulates multiple aspects of reproductive system development. *Developmental biology* **252**, 202-213.

Pathan, M., Keerthikumar, S., Ang, C. S., Gangoda, L., Quek, C. Y., Williamson, N. A., Mouradov, D., Sieber, O. M., Simpson, R. J., Salim, A., et al. (2015). FunRich: An open access standalone functional enrichment and interaction network analysis tool. *Proteomics* **15**, 2597-2601.

Pathan, M., Keerthikumar, S., Chisanga, D., Alessandro, R., Ang, C. S., Askenase, P., Batagov, A. O., Benito-Martin, A., Camussi, G., Clayton, A., et al. (2017). A novel community driven software for functional enrichment analysis of extracellular vesicles data. *J Extracell Vesicles* **6**, 1321455.

Peters, J. M. (2006). The anaphase promoting complex/cyclosome: a machine designed to destroy. *Nat Rev Mol Cell Biol* **7**, 644-656.

Scarpa, E. and Mayor, R. (2016). Collective cell migration in development. *The Journal of cell biology* **212**, 143-155.

Schwarz, E. M., Kato, M. and Sternberg, P. W. (2012). Functional transcriptomics of a migrating cell in Caenorhabditis elegans. *Proceedings of the National Academy of Sciences of the United States of America* **109**, 16246-16251.

Schwendeman, A. R. and Shaham, S. (2016). A High-Throughput Small Molecule Screen for C. elegans Linker Cell Death Inhibitors. *PloS one* **11**, e0164595.

Steeg, P. S., Bevilacqua, G., Kopper, L., Thorgeirsson, U. P., Talmadge, J. E., Liotta, L. A. and Sobel, M. E. (1988). Evidence for a novel gene associated with low tumor metastatic potential. *J Natl Cancer Inst* **80**, 200-204.

Sternberg, P. W. and Horvitz, H. R. (1988). lin-17 mutations of Caenorhabditis elegans disrupt certain asymmetric cell divisions. *Developmental biology* **130**, 67-73.

Su, M., Merz, D. C., Killeen, M. T., Zhou, Y., Zheng, H., Kramer, J. M., Hedgecock, E. M. and Culotti, J. G. (2000). Regulation of the UNC-5 netrin receptor initiates the first reorientation of migrating distal tip cells in Caenorhabditis elegans. *Development* **127**, 585-594.

Sulston, J. E., Albertson, D. G. and Thomson, J. N. (1980). The Caenorhabditis elegans male: postembryonic development of nongonadal structures. *Developmental biology* **78**, 542-576.

Szklarczyk, D., Kirsch, R., Koutrouli, M., Nastou, K., Mehryary, F., Hachilif, R., Gable, A. L., Fang, T., Doncheva, Nadezhda T., Pyysalo, S., et al. (2023). The STRING database in 2023: protein–protein association networks and functional enrichment analyses for any sequenced genome of interest. *Nucleic acids research* **51**, D638-D646.

Tamai, K. K. and Nishiwaki, K. (2007). bHLH transcription factors regulate organ morphogenesis via activation of an ADAMTS protease in C. elegans. *Developmental biology* **308**, 562-571.

Tan, C. H., Park, H. and Sternberg, P. W. (2022). Loss of famh-136/ FAM136A results in minor locomotion and behavioral changes in Caenorhabditis elegans. *MicroPubl Biol* **2022**.

Tran, A. T., Chapman, E. M., Flamand, M. N., Yu, B., Krempel, S. J., Duchaine, T. F., Eroglu, M. and Derry, W. B. (2019). MiR-35 buffers apoptosis thresholds in

the C. elegans germline by antagonizing both MAPK and core apoptosis pathways. *Cell Death Differ* **26**, 2637-2651.
Updike, D. L. and Mango, S. E. (2007). Genetic suppressors of Caenorhabditis elegans pha-4/FoxA identify the predicted AAA helicase ruvb-1/RuvB. *Genetics* **177**, 819-833.
Vogel, B. E. and Hedgecock, E. M. (2001). Hemicentin, a conserved extracellular member of the immunoglobulin superfamily, organizes epithelial and other cell attachments into oriented line-shaped junctions. *Development* **128**, 883-894.
Wang, H., Park, H., Liu, J. and Sternberg, P. W. (2018). An Efficient Genome Editing Strategy To Generate Putative Null Mutants in Caenorhabditis elegans Using CRISPR/Cas9. *G3* **8**, 3607-3616.
Wehman, A. M., Poggioli, C., Schweinsberg, P., Grant, B. D. and Nance, J. (2011). The P4-ATPase TAT-5 inhibits the budding of extracellular vesicles in C. elegans embryos. *Current biology : CB* **21**, 1951-1959.
Wood, W. B., Hecht, R., Carr, S., Vanderslice, R., Wolf, N. and Hirsh, D. (1980). Parental effects and phenotypic characterization of mutations that affect early development in Caenorhabditis elegans. *Developmental biology* **74**, 446-469.
Yochem, J., Weston, K. and Greenwald, I. (1988). The Caenorhabditis elegans lin-12 gene encodes a transmembrane protein with overall similarity to Drosophila Notch. *Nature* **335**, 547-550.
Yoon, S., Kawasaki, I. and Shim, Y. H. (2012). CDC-25.1 controls the rate of germline mitotic cell cycle by counteracting WEE-1.3 and by positively regulating CDK-1 in Caenorhabditis elegans. *Cell cycle* **11**, 1354-1363.
Zambrano, N., Bimonte, M., Arbucci, S., Gianni, D., Russo, T. and Bazzicalupo, P. (2002). feh-1 and apl-1, the Caenorhabditis elegans orthologues of mammalian Fe65 and beta-amyloid precursor protein genes, are involved in the same pathway that controls nematode pharyngeal pumping. *Journal of cell science* **115**, 1411-1422.
Zhou, Y., Zhou, B., Pache, L., Chang, M., Khodabakhshi, A. H., Tanaseichuk, O., Benner, C. and Chanda, S. K. (2019). Metascape provides a biologist-oriented resource for the analysis of systems-level datasets. *Nature communications* **10**.

Fig 1. Surface overexpression of ITFG1 in MDA-MB-231 cells. ITFG1-Myc-expressing MDA-MB-231 cells and non-expressing control cells were harvested at 48 h post transient transfection for determining ITFG1 expression. (A) ITFG1 RNA in cell lysates was quantified by real-time PCR. Data show ITFG1 RNA levels relative to GAPDH. Two individual transfections were analyzed. Error bars represent SD (n = 3). (B) Representative western blot images showing the expression of ITFG1 and GAPDH (loading control) in cell lysates. ITFG1 expression was probed with anti-Myc (left) or anti-

ITFG1 antibodies (right). (C) Subcellular fractions of cells lysates were collected for determining the expression location of ITFG1 or ITFG1-Myc by western blot using anti-ITFG1 antibody. (D) Cells were immunofluorescence stained for the presence of ITFG1 using anti-ITFG1 antibody (Red). Hoechst was used for nuclear staining (Blue). (E) Surface expression of ITFG1 was examined by flow cytometry after staining the cells with anti-ITFG1 antibody.

Fig 2. ITFG1-RUVBL1 interaction in ITFG1-expressing MDA-MB-231 cells. Immunoprecipitates from ITFG1-Myc transient or stably expressing MDA-MB-231 cells using anti-Myc agarose were subjected to LC/MS-MS analysis for (A) ITFG1 protein level and (B) RUVBL1 protein level. Data show fold change of the protein level in Log2 between ITFG1-Myc-expressing cells over non-expressing control MDA-MB-231 cells. FC, fold change. Immunoprecipitation was performed in biological triplicate. (C) Western blot assay identified ITFG1 and RUVBL1 in Myc-immunoprecipitates in ITFG1-Myc transient expressing cells using anti-Myc and anti-RUVBL1 antibodies, respectively. (D) ITFG1-Myc stably expressing or non-expressing control MDA-MB-231 were transient transfected with FLAG-RUVBL1 expression plasmid. Cells were harvested at 48 h post-transfection and procced to immunoprecipitation using anti-FLAG beads. Western blot assay identified ITFG1 and RUVBL1 in FLAG-immunoprecipitates in FLAG-RUVBL1 transient expressing cells using anti-ITFG1 and anti-FLAG antibodies, respectively. (C, D) Input from cells was used as positive control. GAPDH was used as loading control for input and negative control for immunoprecipitation. IP, immunoprecipitation.

Fig 3. Function and pathway analysis of ITFG1 interactors. (A, B) Graph represents ITFG1 interactors identified by LC/MS-MS. Immunoprecipitates from ITFG1-Myc transient or stably expressing MDA-MB-231 cells were compared to non-expressing control MDA-MB-231 cells. Data show fold change of the protein level in Log2 between ITFG1-Myc-expressing cells over non-expressing control MDA-MB-231 cells. FC, fold change. Each dot represents one protein. Red indicates ITFG1. (B) Set of proteins that were upregulated in ITFG-Myc-expressing cells compared to non-expressing control MDA-MB-

231 cells were identified (|log2 FC| > 2). Venn plots shows the upregulated protein numbers identified in ITFG1-Myc transient and stably expressing MDA-MB-231 cells. (C) Reactome pathway and GO biological process enrichment of the overlapping 180 proteins in ITFG-Myc expressing MDA-MB-231 cells. Data present the top 20 statistically enriched terms (*P*-adjusted value < 0.05).

Fig. 4 Mutations in the orthologs of ITFG1 interactors resulted in phenotypes similar to that of *lnkn-1* mutants. (A) Homozygotic animals of lethal/ sterile mutations used in this study descended from balanced heterozygotic mothers. Homozygotic animals were identified through the lack of fluorescently labeled balancers (green in the cartoon). In the maternal effect experiments, the homozygotic hermaphrodites were mated with wild-type males carrying a fluorescent genetic marker (*oxTi719* [*eft-3p::tdTomato::H2B*]) (Frokjaer-Jensen et al., 2014). (B) LNKN-1 is required maternally. Heterozygotic cross-progenies of *lnkn-1(sy1596)* hermaphrodites and *lnkn-1(+/+)* males fail to develop and die without hatching (The embryos carrying the orange-colored male-derived *oxTi719* marker can be seen). (C) Phenotypical analysis of the orthologs of ITFG1 interactors in *C. elegans*. Phenotype 2 and 5 was defined by having F_1 progenies that hatch; Phenotype 3 was defined by embryos/ embryo-like objects or oocytes observed outside of the unmated hermaphrodite. Embryos and, in particular, oocytes may not be completely absent in all animals. This was especially the case in *unc-94(ok1210)*. Some *rod-1(tm6186)* animals also produce oocytes and embryo-like objects. Phenotype 4 was defined by the observation of F_1 embryos/animals carrying the male-derived *oxTi719* marker. *: Very rarely; #: maternal effect sterile.

Fig. 5 Potential LNKN-1 interactors displayed a similar gonad migration phenotype in hermaphrodites. (A-B). Loss of *lnkn-1* resulted in premature stopping of gonad migration in hermaphrodites (A) *lnkn-1(+)* control. (B) *lnkn-1(sy1596)* worms have a shortened dorsal-distal half of the gonad. (C-D) The premature stopping phenotype is defined by comparing the value of Centripetal migration (%) of the mutants to that of the wild-type (N2). The Centripetal migration (%) is determined by the ratio of dorsal-distal

gonad arm length to that of ventral-proximal gonad arm length. The arm lengths were approximated as the distance from the vulval to the ventral-dorsal turn of the U-shaped gonad for the ventral-proximal gonad arm length; and the distance from the distal end of the gonad to the ventral-dorsal turn for the dorsal-distal gonad arm length. See materials and methods for detail. (D) Examination of gonad migration in hermaphrodites. Mutation in some of the candidate genes also causes pathfinding or other gonadal development defects in a number of animals. For the purpose of this examination, only gonads that made the centripetal migration was included. The pathfinding effects were consistently observed in *cdc-25.1(ok1888)* and *rod-1(tm6186)* and occurred at a lower frequency in *tat-5(tm1741)* and *apc-2(ok1657)* mutant animals. *rod-1(tm6186)* animals were also observed to have missing gonad arms (n≥10. All comparisons were with the wild-type, **: p<0.01, ***: p<0.001, ****: p<0.0001, Student's *t*-test).

Fig. 6 TAT-5/ATP9A, NDK-1/NME1, and APC-2/ANAPC2 are required for the integrity of the migrating male nematode gonad. (A) Males homozygotic for *tat-5(tm1741)*, *ndk-1(ok314)*, *apc-2(ok1657)*, and *lin-40(gk255)* have gonads that were not connected to the exterior similar to that of *lnkn-1(sy1596)*. For each genotype, the controls were siblings carrying the genetic balancer and were either the wild-type or heterozygous for the locus (n≥19, ****: p<0.0001, chi-square test). (B-E) Detached linker cells (LC) were found in males carrying *tat-5(tm1741)*, *ndk-1(ok314)*, or *apc-2(ok1657)*, similar to that of *lnkn-1(sy1596)*. Images are of animals in the L4 larvae stage, with *lag-2p::YFP* (syIs128) (colored in green) labeling the detached linker cell (LC). The posterior end of the remaining gonad is outlined in a white dashed line. (B) *lnkn-1(sy1596)*. (C) *tat-5(tm1741)*. (D) *ndk-1(ok314)*. (E) *apc-2(ok1657)*.

Fig. S1. ITFG1 identification from in-gel digestion. (A) Coomassie blue staining of SDS-PAGE for Myc-immunoprecipitates from ITFG1-Myc expressing and non-expressing control MDA-MB-231 cells. Gel lanes in the molecular weight range between 150 and 250 kDa (R1), 75 and 150 kDa (R2), and 37 and 75 kDa (R3) were removed followed by in-gel digested for LC/MS-MS analysis. (B) ITFG1 protein abundance in each region.

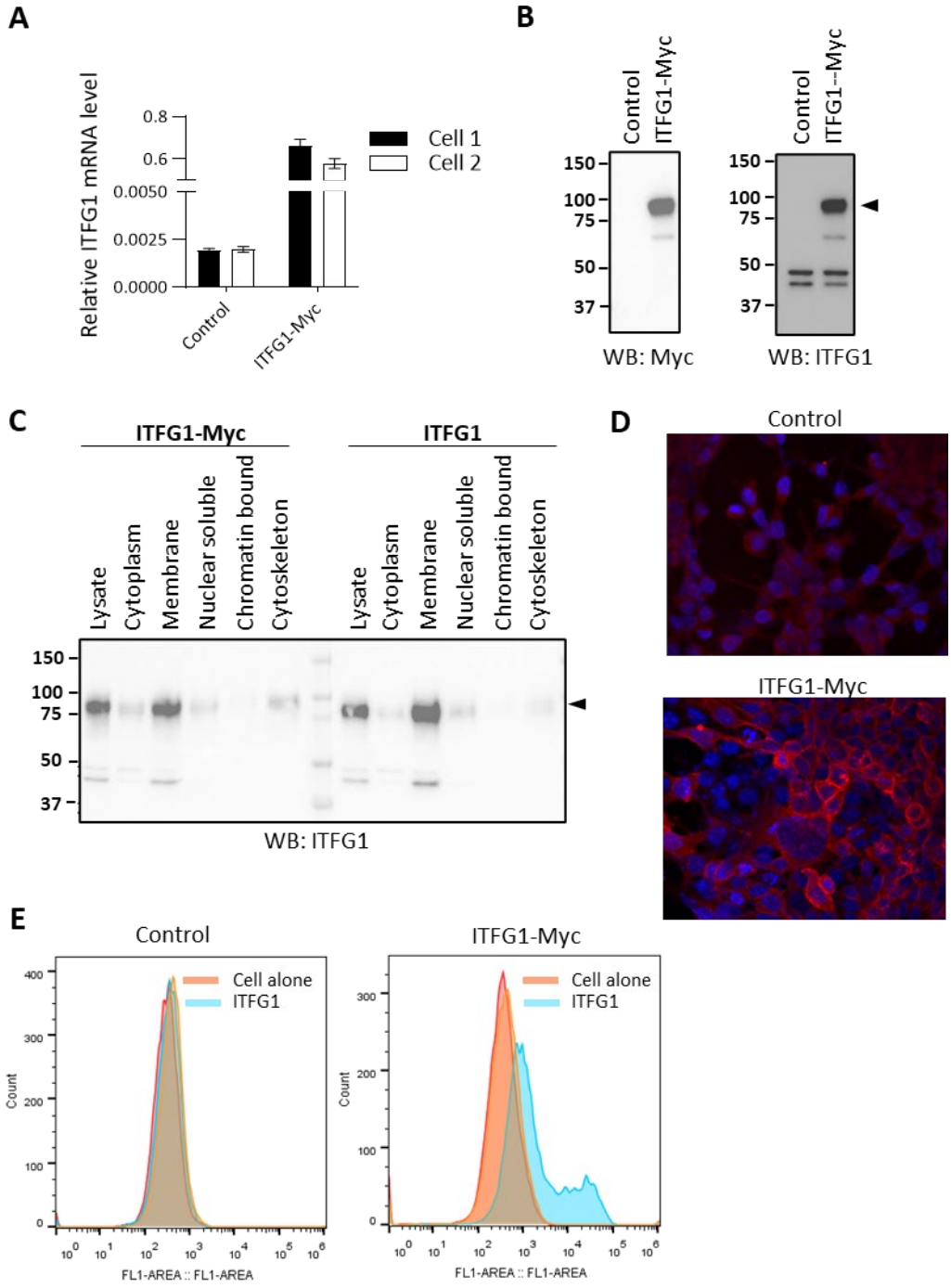
A
Relative ITFG1 mRNA level
0.8
0.6
0.0050
0.0025
0.0000
Control
ITFG1-Myc
Cell 1
Cell 2
B
Control
ITFG1-Myc
150
100
75
50
37
WB: Myc
WB: ITFG1
C
ITFG1-Myc
ITFG1
Lysate
Cytoplasm
Membrane
Nuclear soluble
Chromatin bound
Cytoskeleton
WB: ITFG1
D
Control
ITFG1-Myc
E
Control
ITFG1-Myc
Cell alone
ITFG1
Count
FL1-AREA :: FL1-AREA

Fig. 1

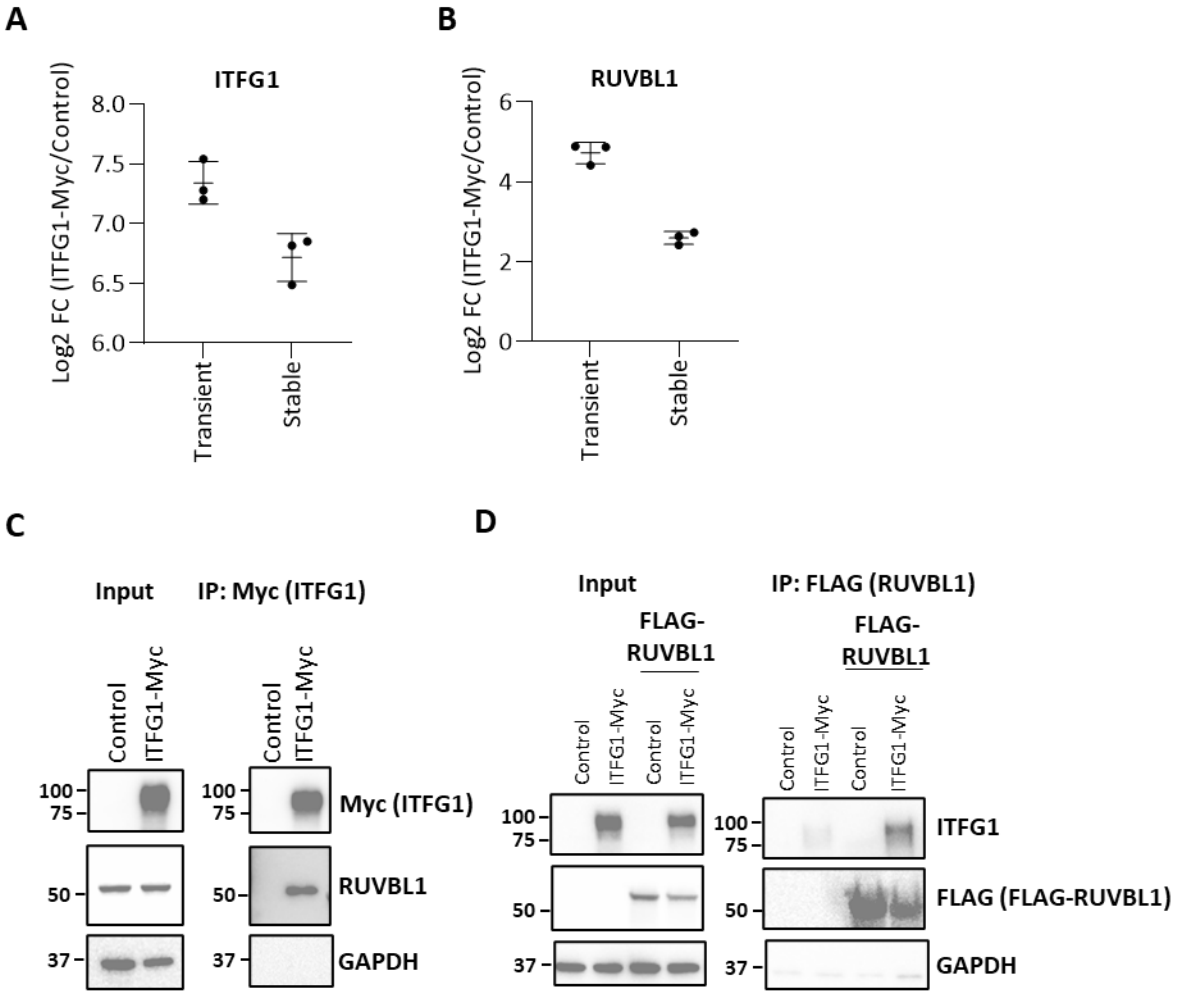
A
ITFG1
Log2 FC (ITFG1-Myc/Control)
8.0
7.5
7.0
6.5
6.0
Transient
Stable
B
RUVBL1
Log2 FC (ITFG1-Myc/Control)
6
4
2
0
Transient
Stable
C
Input
IP: Myc (ITFG1)
Control
ITFG1-Myc
Control
ITFG1-Myc
100
75
50
37
Myc (ITFG1)
RUVBL1
GAPDH
D
Input
IP: FLAG (RUVBL1)
FLAG-RUVBL1
FLAG-RUVBL1
Control
ITFG1-Myc
Control
ITFG1-Myc
Control
ITFG1-Myc
Control
ITFG1-Myc
100
75
50
37
ITFG1
FLAG (FLAG-RUVBL1)
GAPDH

Fig. 2

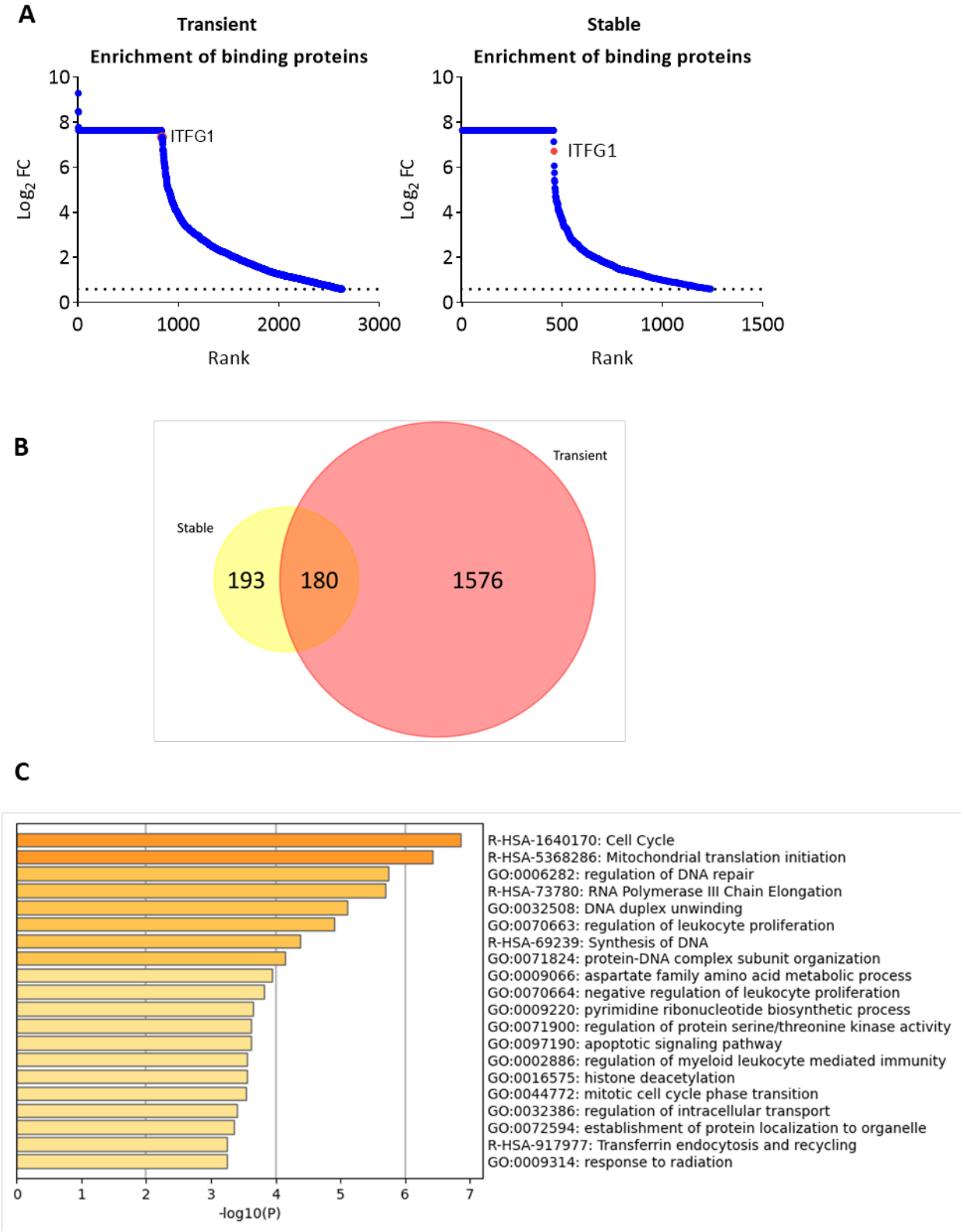
A
Transient
Enrichment of binding proteins
ITFG1
Log2 FC
Rank
Stable
Enrichment of binding proteins
ITFG1
Log2 FC
Rank
B
Transient
Stable
193
180
1576
C
R-HSA-1640170: Cell Cycle
R-HSA-5368286: Mitochondrial translation initiation
GO:0006282: regulation of DNA repair
R-HSA-73780: RNA Polymerase III Chain Elongation
GO:0032508: DNA duplex unwinding
GO:0070663: regulation of leukocyte proliferation
R-HSA-69239: Synthesis of DNA
GO:0071824: protein-DNA complex subunit organization
GO:0009066: aspartate family amino acid metabolic process
GO:0070664: negative regulation of leukocyte proliferation
GO:0009220: pyrimidine ribonucleotide biosynthetic process
GO:0071900: regulation of protein serine/threonine kinase activity
GO:0097190: apoptotic signaling pathway
GO:0002886: regulation of myeloid leukocyte mediated immunity
GO:0016575: histone deacetylation
GO:0044772: mitotic cell cycle phase transition
GO:0032386: regulation of intracellular transport
GO:0072594: establishment of protein localization to organelle
R-HSA-917977: Transferrin endocytosis and recycling
GO:0009314: response to radiation
-log10(P)

Fig. 3

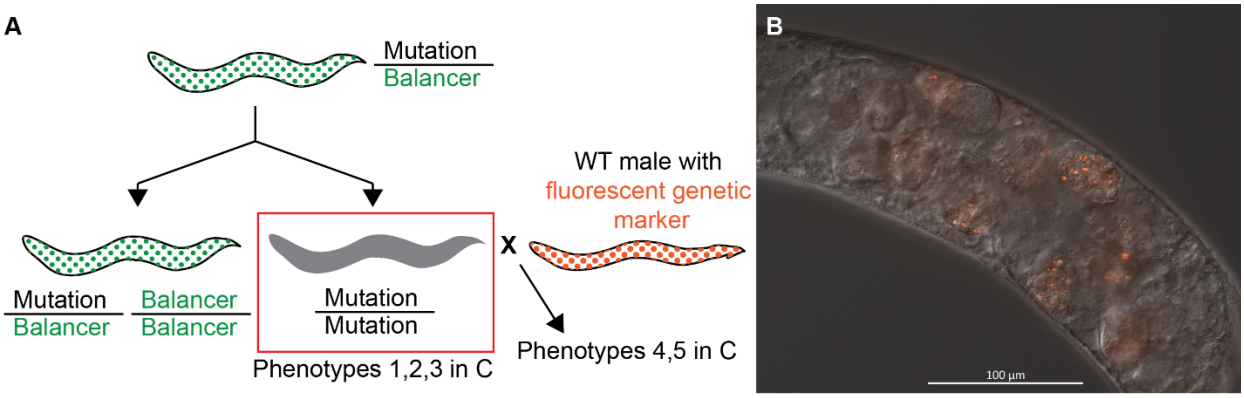

C

			Hermaphrodite phenotypic analysis				
	Phenotypes		1	2	3	4	5
Human Protein	**Worm ortholog**	**Allele**	**Develop to adults?**	**Produce live progenies**	**Lay oocyte or embryos**	**Observed cross-fertilization**	**Viable mated progenies**
ITFG1	*lnkn-1*	*sy1596*	Y	N	Y	Y	N
LMOD3	*unc-94*	*ok1210*	Y	N	N*	Y	Y
CDC25C	*cdc-25.1*	*ok1888*	Y	N	N	N	N
ATP9A	*tat-5*	*tm1741*	Y	N	Y	Y	N
NME1/4	*ndk-1*	*ok314*	Y	N	N	N	N
APBB1	*feh-1*	*gb561*	N	-	-	-	-
MVK	*mvk-1*	*tm6628*	N	-	-	-	-
TTC27	*trd-1*	*tm2764*	N	-	-	-	-
ANAPC2	*apc-2*	*ok1657*	Y	N	N	N	N
ATP6AP1	*vha-19*	*tm2225*	N	-	-	-	-
KNTC1	*rod-1*	*tm6186*	Y	N	N	N	N
RAD51	*rad-51*	*ok2218*	Y	N	Y	N	N
HSPA2	*hsp-1*	*ok1371*	N	-	-	-	-
CDC25C	*cdc-25.2*	*ok597*	Y	Y	-	-	-
MTA2	*lin-40*	*gk255*	Y	Y#	-	-	-
GNB1L	*C10B5.1*	*ok3270*	Y	N	Y	Y	N
HSP90AB4P	*hsp-90*	*ok1333*	N	-	-	-	-
VPS41	*vps-41*	*ok3433*	Y	N	Y	N	N

Fig. 4

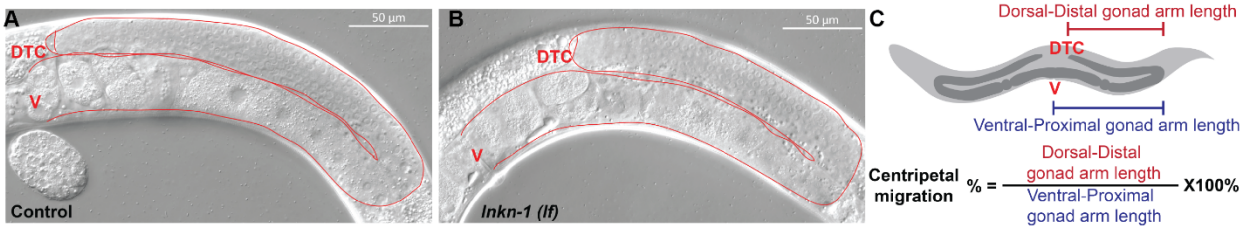

D

Genes	Anterior Ventral-Proximal Gonad arm length (µm)	Posterior Ventral-Proximal Gonad arm length (µm)	Anterior centripetal migration (%)	Posterior centripetal migration (%)
WT	477.6±44.2 (n= 21)	432.7±39.7 (n= 24)	88.6±7.7 (n= 21)	98.1±7.6% (n= 24)
lnkn-1	296.7±31.3 (n= 28)****	272.2±26.3 (n= 27)****	69.9±12.4% (n= 28)****	67.4±19.5% (n= 27)****
unc-94	392.2±50.1 (n= 10)***	356.6±50.3 (n= 14)****	93.7±10.3% (n= 10, N.D.)	96.4±11.6% (n= 14, N.D.)
cdc-25.1	217.1±22.0 (n= 13)****	224.3±16.7 (n= 17)****	39.4±12.3% (n= 13)****	42.5±10.9% (n= 17)****
tat-5	180.2±29.4 (n= 15)****	177.9±21.0 (n= 14)****	59.4±13.4% (n= 15)****	54.1±18.1% (n= 14)****
ndk-1	235.3±33.1 (n= 14)****	208.7±34.1 (n= 13)****	44.0±16.9% (n= 14)****	54.2±16.0% (n= 13)****
apc-2	187.0±29.5 (n= 18)****	174.1±33.1 (n= 18)****	58.7±15.4% (n= 18)****	42.3±15.1% (n= 18)****
rod-1	240.6±28.8 (n= 15)****	246.7±34.4 (n= 11)****	91.6±24.5% (n= 15, N.D.)	84.9±42.7% (n= 11, N.D.)
rad-51	431.4±35.2 (n= 19)***	372.5±17.4 (n= 10)****	90.2±9.4% (n= 19, N.D.)	105.0±5.7% (n= 10)**
C10B5.1	194.3±30.5 (n= 12)****	176.5±33.6 (n= 17)****	47.7±20.4% (n= 12)****	59.7±21.2% (n= 17)****
vps-41	273.3±56.7 (n= 11)****	237.7±56.7 (n= 10)****	88.4±17.4% (n= 11, N.D.)	103.2±7.4% (n= 10, N.D.)

**: $P<0.01$; ***: $P<0.001$; ****: $P<0.0001$

Fig. 5

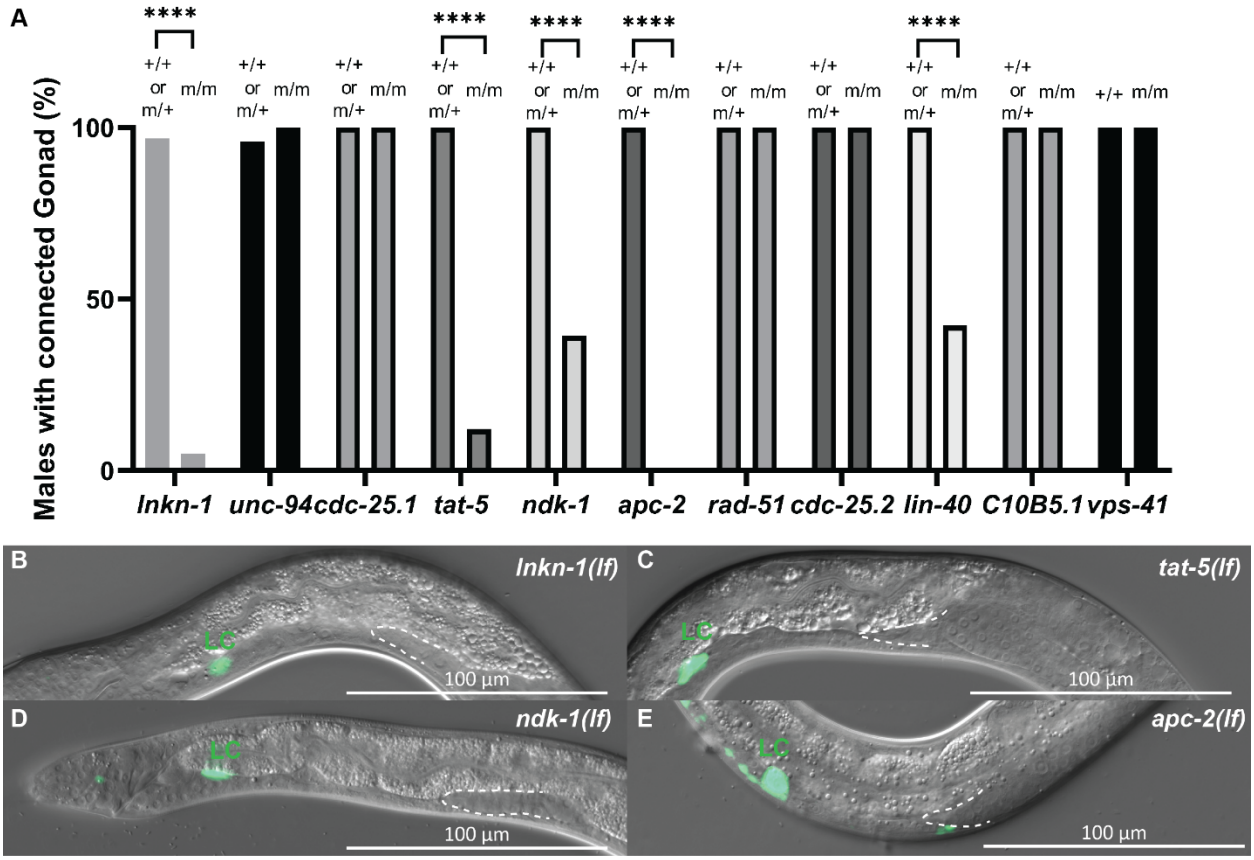
A
****
+/+ or m/+
m/m
Males with connected Gonad (%)
100
50
0
lnkn-1
unc-94
cdc-25.1
tat-5
ndk-1
apc-2
rad-51
cdc-25.2
lin-40
C10B5.1
vps-41
B
lnkn-1(lf)
C
tat-5(lf)
D
ndk-1(lf)
E
apc-2(lf)
LC
100 µm

Fig. 6